catalysts

MDPI

Article

Flexibility and Function of Distal Substrate-Binding Tryptophans in the Blue Mussel β-Mannanase *Me*Man5A and Their Role in Hydrolysis and Transglycosylation

Simon Birgersson [1], Johan Morrill [1], Olof Stenström [2], Mathias Wiemann [1], Ulrich Weininger [2,†], Pär Söderhjelm [2], Mikael Akke [2] and Henrik Stålbrand [1,*]

[1] Biochemistry and Structural Biology, Department of Chemistry, Lund University, P.O. Box 124, S-221 00 Lund, Sweden; simon.birgersson@biochemistry.lu.se (S.B.); johan.morrill@gmail.com (J.M.); mathias.wiemann@biochemistry.lu.se (M.W.)

[2] Biophysical Chemistry, Department of Chemistry, Lund University, P.O. Box 124, S-221 00 Lund, Sweden; olof.stenstrom@saromics.com (O.S.); ulrich.weininger@physik.uni-halle.de (U.W.); par.soderhjelm@bpc.lu.se (P.S.); mikael.akke@bpc.lu.se (M.A.)

* Correspondence: henrik.stalbrand@biochemistry.lu.se; Tel.: +46-46-2228202

† Present address: Institute of Physics, Biophysics, Martin-Luther-University Halle-Wittenberg, D-06108 Halle (Saale), Germany.

Abstract: β-Mannanases hydrolyze β-mannans, important components of plant and microalgae cell walls. Retaining β-mannanases can also catalyze transglycosylation, forming new β-mannosidic bonds that are applicable for synthesis. This study focused on the blue mussel (*Mytilus edulis*) GH5_10 β-mannanase *Me*Man5A, which contains two semi-conserved tryptophans (W240 and W281) in the distal subsite +2 of its active site cleft. Variants of *Me*Man5A were generated by replacing one or both tryptophans with alanines. The substitutions reduced the enzyme's catalytic efficiency (k_{cat}/K_m using galactomannan) by three-fold (W281A), five-fold (W240A), or 20-fold (W240A/W281A). Productive binding modes were analyzed by ^{18}O labeling of hydrolysis products and mass spectrometry. Results show that the substitution of both tryptophans was required to shift away from the dominant binding mode of mannopentaose (spanning subsites −3 to +2), suggesting that both tryptophans contribute to glycan binding. NMR spectroscopy and molecular dynamics simulations were conducted to analyze protein flexibility and glycan binding. We suggest that W240 is rigid and contributes to +2 subsite mannosyl specificity, while W281 is flexible, which enables stacking interactions in the +2 subsite by loop movement to facilitate binding. The substitutions significantly reduced or eliminated transglycosylation with saccharides as glycosyl acceptors but had no significant effect on reactions with alcohols.

Keywords: β-mannanase; enzymatic synthesis; transglycosylation; flexibility; novel glycosides

Citation: Birgersson, S.; Morrill, J.; Stenström, O.; Wiemann, M.; Weininger, U.; Söderhjelm, P.; Akke, M.; Stålbrand, H. Flexibility and Function of Distal Substrate-Binding Tryptophans in the Blue Mussel β-Mannanase *Me*Man5A and Their Role in Hydrolysis and Transglycosylation. *Catalysts* **2023**, *13*, 1281. https://doi.org/10.3390/catal13091281

Academic Editors: Teodora Bavaro and Giovanna Speranza

Received: 7 August 2023
Revised: 1 September 2023
Accepted: 2 September 2023
Published: 7 September 2023

1. Introduction

Endo-β-1,4-D-mannanases (β-mannanases, EC 3.2.1.78) are glycoside hydrolases (GHs) found in a wide variety of organisms that utilize various common β-mannan-based polysaccharides [1] and are the major depolymerizing enzyme type involved in β-mannan degradation. They catalyze the hydrolysis of β-1,4-mannosidic bonds within the β-mannan backbone and have, to date, been classified according to sequence similarity [2] into GH families GH5, GH26, GH113, and GH134 as displayed in the Carbohydrate-Active enZYmes (CAZy) database (http://www.cazy.org) (accessed on 7 August 2023) [3]. GH5, GH26, and GH113 enzymes belong to the large GH clan A of (α/β)8 barrel-folded members. Within GH5, β-mannanases have been further classified into subfamilies GH5_7, GH5_8, GH5_10, and a few into the GH5_17 subfamily [4]. GH5 and GH26 β-mannanases possess two conserved catalytic glutamates (nucleophile and acid/base) which are involved in the retaining

double-displacement mechanism [5]. The nucleophile attacks the anomeric carbon, resulting in the formation of a covalent glycosyl–enzyme intermediate. This intermediate is then attacked by a water molecule, leading to hydrolysis and release of the carbohydrate moiety. In addition to hydrolysis, β-mannanases may be capable of catalyzing transglycosylation reactions where another molecule (glycosyl acceptor) is used instead of water to attack the covalent intermediate (glycosyl donor). The acceptor is thus conjugated with the donor, resulting in the formation of a new glycoside [6]. Several GH5 β-mannanases have been shown to catalyze transglycosylation with, e.g., saccharides or alcohols as acceptors [7–10], while GH26 β-mannanases are not known for significant transglycosylation capacity [11,12]. β-Mannans are abundant in nature, notably in the form of softwood hemicellulose [13], seed galactomannan [14], and certain algae [15]. There is an increased interest in the use of the transglycosylating capacity of retaining GHs for enzyme-catalyzed synthesis of glycosides, e.g., alkyl glycosides used as environmentally friendly surfactants [16] or ethyl-methacrylate glycosides used to generate novel polymers [17]. In this regard, retaining β-mannanases have great potential for the conversion of renewable, but currently essentially unexploited, mannans into novel biochemicals. We recently demonstrated such a route by β-mannanase-catalyzed synthesis of hexyl mannosides with shown surfactant properties [18].

β-Mannanases and other endo-acting GHs have several glycosyl-binding subsites, where each binds one glycosyl monomer unit. Subsites are numbered from negative to positive integer steps. Positively numbered (herein termed aglycone) subsites are located toward the reducing end of the substrate, and negatively numbered (glycone) subsites toward the non-reducing end [6]. The glycosidic bond connecting monomers bound in subsites −1 and +1 is cleaved. The covalent glycosyl–enzyme intermediate is formed in the −1 subsite, which is usually highly conserved within each GH family. In transglycosylation, acceptors are thus expected to be accommodated in the aglycone (+) subsites, where sequence conservation is lower. The GH5 subfamily 7 (GH5_7) contains bacterial and eukaryotic β-mannanases [4,8,19]. The +1 and +2 subsites have been indicated to play a significant role in hydrolysis and transglycosylation in several fungal GH5_7 β-mannanases [7,8,10] as well as in other GHs, such as a GH11 xylanase [20], GH18 chitin-acting enzymes [21], and others [22]. Lowered glycan interaction due to mutation(s) in this region may be beneficial for transglycosylation with non-saccharide acceptors, as investigated for the synthesis of allyl mannosides by the GH5_7 β-mannanase *Tr*Man5A [9]. Sequence-based protein engineering aiming at transglycosylation yield enhancement of a GH2 β-mannosidase and other enzymes across several GH families has successfully been developed [23]. A mechanistic explanation for such improvements, however, is still unclear in most cases, motivating further structure-function elucidation of relevance for the transglycosylation efficiency of GHs.

β-Mannanases are not only produced by microbes [1] but also by higher organisms, with examples such as the GH5_10 β-mannanase from *Eisenia fetida* [24], or transglycosylating GH5_7 enzymes from plants [19,25]. Furthermore, the blue mussel *Mytilus edulis* secretes the subfamily GH5_10 β-mannanase *Me*Man5A into its crystalline style [26–29]. The crystalline style is a hard rod-like structure in the stomachs of mollusks that is involved in diet digestion and contains several types of GHs [30]. Previous studies have indicated that *Me*Man5A is capable of transglycosylation with saccharides as acceptors [26,29]. Structural analysis of *Me*Man5A indicates at least six sugar-binding subsites. In the +2 subsite of *Me*Man5A, two tryptophans (W240 and W281, 10.3 Å apart) are positioned such that they could possibly interact with mannosyl units, but this has not been investigated previously [29] (Figure 1A). The architecture of the +2 subsite differs significantly from fungal and bacterial β-mannanases, which mainly belong to subfamilies GH5_7 and GH5_8, respectively. W281 is situated in loop 6, located between the sixth barrel β-strand and α-helix (residues 277–295) [29], that may be flexible as indicated by the comparably high B-factors of W281 [29]. It was hypothesized that movement of the W281 side-chain could be required for interactions with a mannosyl unit in subsite +2 (Figure 1A). However, the significance

of W240 and W281 in possible glycan interactions has not yet been established. These two tryptophans are semi-conserved, present in the majority (approx. 70%) of eukaryotic GH5_10 β-mannanases as analyzed by multiple sequence alignment and displayed in crystal structures [24,29,31,32] (Figure 1A).

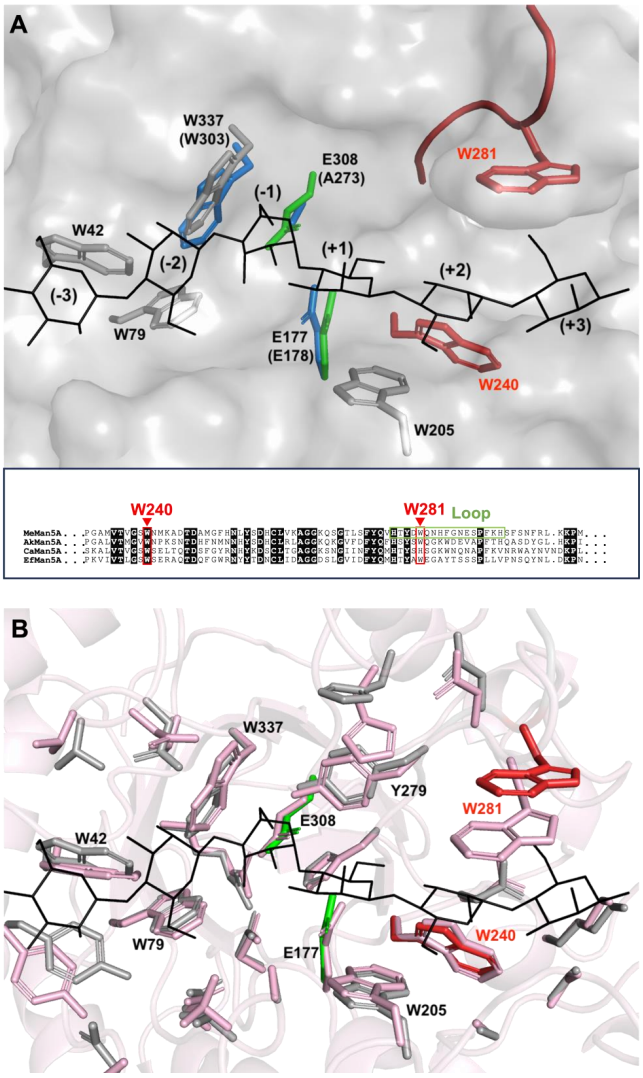

Figure 1. The active site cleft of *Me*Man5A. (**A**) Structural superimposition between the (apo) *Me*Man5A crystal structure (PDB: 2C0H) [29] using the nucleophile substituted E273A variant of the GH5_8 beta-mannanase StMandC co-crystallized with mannohexaose (ligand in black) (PDB: 4Y7E). The surface of *Me*Man5A is shown in light gray with the catalytic nucleophile (E308) and acid/base (E177) in green stick representation. *Me*Man5A Tryptophan side-chains within 3 Å of the ligand shown in stick representation (W240 and W281 in red). W337, E308, and E177 are conserved with StMandC (blue residues, numbering in brackets). (**Insert**) Selected section of a structure-based multiple sequence alignment of the GH5_10 β-mannanases *Me*Man5A (PDB: 2C0H) [29], AkMan5A (PDB: 3VUP) [31], CaMan5A (PDB: 4OOU) [32], and EfMan5A (PDB: 5Y6T) [24]. Residues conserved in all three structures are in bold. The positions corresponding to W240 and W281 in *Me*Man5A are indicated with red boxes and arrows. Loop 6 (residues 277–295 in *Me*Man5A) that harbors W281 is boxed in green. The alignment was carried out using Clustal Omega (www.ebi.ac.uk/, accessed on 14 June 2023). (**B**) Structural superimposition of the *Me*Man5A apo crystal structure (grey, W281/W240 red, catalytic residues green) with a representative snapshot of the simulated mannohexaose (M_6)-complex in pink. M_6 is in black. W281 changes position in comparison to the apo structure (~2.7 Å) when the ligand is bound during the duration of the 70 ns simulation.

In the present paper, we study W240 and W281 in the +2 subsite of *Me*Man5A with the aim of elucidating their potential roles in hydrolysis and transglycosylation. In addition, we analyze the enzyme's transglycosylation potential and applicability in enzymatic synthesis of novel compounds. To do this, we created mutated variants of *Me*Man5A where either W240, W281, or both tryptophans were replaced with alanines. We evaluated the effect of these substitutions on enzyme kinetics, product profiles, and subsite binding, as well as transglycosylation with saccharides and alcohols as acceptors. Using NMR spectroscopy and molecular dynamic (MD) simulation, we characterized the flexibility and glycan interactions of, in particular, W281. The results show that both W240 and W281 affect the catalytic efficiency of *Me*Man5A and furthermore suggest different roles of these two tryptophans.

2. Results

2.1. Basic Enzyme Characterization

The wild type (WT) GH5_10 β-mannanase from *Mytilus ediulis* (*Me*Man5A) and its three mutated variants (W240A, W282A, and W240A/W281A) were recombinantly expressed in *Pichia* and purified. The enzymes were characterized for activity using an assay with locust bean galactomannan (LBG) as substrate and detection of reducing sugars by 3,5-dinitrosalicylic acid (DNS). The specific β-mannanase activity using LBG was 253 ± 6 (WT *Me*Man5A), 87 ± 8 (W240A), 107 ± 2 (W281A), and 39 ± 18 (W240A/W281A) kat/mol, respectively. The pH optimum of WT *Me*Man5A was determined to be pH 5.2 in 50 mM sodium citrate buffer, in line with previous studies [26]. W240A and W281A also had pH optima of pH 5.2, while W240A/W281A had a pH optimum at pH 5.0 but retained >90% of maximal activity at pH 5.2, and this pH was routinely used for incubations. The stability of the enzymes was determined by analyzing the retained activity after storage at 40 °C in 50 mM sodium citrate buffer (pH 5.2) and 0.1 g/L bovine serum albumin (BSA). WT *Me*Man5A, as well as the W281A and W240A mutants, showed fully retained activity after 4 h whilst the W281A/W240A double mutant showed ~40% retained activity. After 24 h, both WT and W281A *Me*Man5A showed fully retained activity, W240A showed slightly reduced activity (~85% remaining), and the double mutant showed significant activity loss (~20% remaining).

2.2. Hydrolysis and Transglycosylation Product Formation

Product formation from incubations with manno-oligosaccharides was analyzed by high-performance anion-exchange chromatography with pulsed amperometric detection (HPAEC-PAD). The major products of mannopentaose (M_5) degradation by WT *Me*Man5A, W240A, and W281A were mannobiose (M_2) and mannotriose (M_3), followed by mannotetraose (M_4) and mannose (M_1). By contrast, W240A/W281A formed approximately equal amounts of M_1, M2, M_3, and M_4 (Table 1). Significantly higher amounts of M_4 compared to M_1 are produced by WT *Me*Man5A with an M_4:M_1 ratio of 6.2 (Table 1). Such unequal formation of two oligosaccharide products, which together correspond to the same degree of polymerization (DP) as the original substrate (in this case, M_5), indicates that transglycosylation products have been formed and then subjected to secondary hydrolysis [26,29]. W240A and W281A gave an M_4:M_1 ratio of 1.8, indicating significantly lower transglycosylation capacity than WT *Me*Man5A (product ratio 6.2) (Table 1). W240A/W281A exhibits a ratio of 1.0 (Table 1), indicating that hydrolysis only occurred and complete loss of transglycosylation capacity [33].

Table 1. Quantification of products from conversion of 1 mM M_5 incubated at 40 °C and pH 5.2 with WT *Me*Man5A (45 min), W240A (30 min), W281A (30 min) and W240A/W281A (15 min) at a similar degree of M_5 conversion (20–30%). The ratio of M_4 to M_1 for each enzyme variant is listed.

Product	WT	W240A	W281A	W240A/W281A
[M_1] (μM)	7.7 ± 0.1	36 ± 0.6	8.7 ± 0.1	89 ± 0.9
[M_2] (μM)	183 ± 1	153 ± 2	235 ± 0.4	82 ± 0.9
[M_3] (μM)	191 ± 0.8	163 ± 3	251 ± 0.6	96 ± 1
[M_4] (μM)	48 ± 0.4	64 ± 1	16 ± 0.9	89 ± 1
[M_4]: [M_1] ratio	6.2	1.8	1.8	1.0

In agreement with the calculated product ratios above, transglycosylation products (DP 7–8) were indeed captured by matrix-assisted laser desorption/ionization time-of-flight mass spectrometry (MALDI-TOF MS), analysis of the reactions with WT *Me*Man5A incubated with M_5 (Figure 2A), as well as with W240A and W281A. However, no such products were detected with W240A/W281A (Figure 2B). Thus, either W240 or W281 in the +2 subsite of *Me*Man5A appears to be required for transglycosylation with saccharides as acceptors. WT *Me*Man5A was also able to use digalactosylated mannopentaose (G_2M_5) as an acceptor, as deduced from the detection of ^{18}O-labeled DP9 and DP10 oligosaccharides when incubated with M_5 and ^{18}O-labeled G_2M_5 (Figure 2C). Thus, this enzyme is interesting for the synthesis of complex saccharides. A control reaction without G_2M_5 as an acceptor did not generate such products (Figure S1). G_2M_5 was inert to hydrolysis by WT *Me*Man5A as analyzed with HPAEC-PAD, possibly due to steric hindrance provided by the galactose side groups.

MALDI-TOF MS product analysis showed that *Me*Man5A can also use alcohols as acceptors, enhancing the potential of the enzyme for synthetic applications. Using WT *Me*Man5A incubated with M_5 and either 5% (*v*/*v*) methanol, propargyl alcohol, or hexanol, we detected as products methyl mannosides, propargyl mannosides, or hexyl mannosides, respectively (Figures 3 and S2). Reactions with methanol and hexanol were also set up using W240A and W281A (Figure 3). Interestingly, no obvious differences in alkyl mannoside production can be observed between WT *Me*Man5A, W240A, and W281A, suggesting that the W240A and W281A substitutions in the +2 subsite do not significantly affect the ability to use alcohols as acceptors.

2.3. Productive Binding Mode Preferences

MALDI-TOF MS analysis of M_5 hydrolysis in ^{18}O-water provided further insight into productive substrate-binding. WT *Me*Man5A, W240A, and W281A preferred binding M_5 from subsite −3 to +2 (Figure 4), suggesting significant productive mannose-unit binding in the +2 subsite is retained despite substituting either W240 or W281. The W281A substitution did not affect binding modes, while a minor shift was observed with W240A (Figure 4), explaining the generation of more M_1 and M_4 by W240A (Table 1). With W240A/W281A, the preference for binding M_5 from subsite −3 to +2 is lost, and M_5 binding from subsite −4 to +1 becomes equally frequent (Figure 4), possibly due to reduced favorable mannosyl interaction in the +2 subsite.

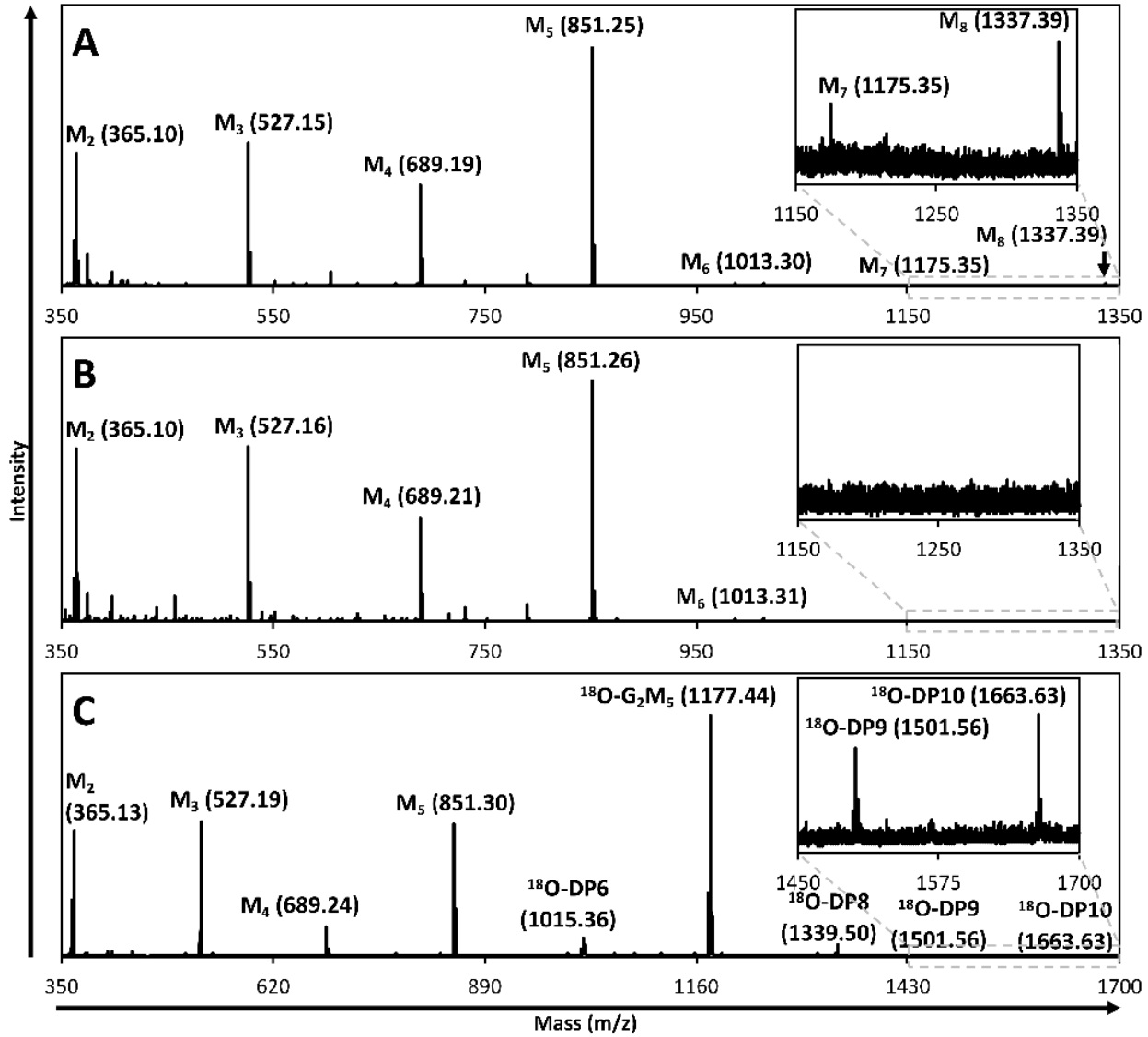

Figure 2. MALDI-TOF MS spectra of reactions with WT *Me*Man5A, W240A/W281A, and M_5. 5 mM M_5 was incubated for 5 h at 40 °C and 20 mM NaAc pH 5.2 using WT *Me*Man5A (**A**), and the W240A/W281A variant of *Me*Man5A (**B**). (**C**) Spectra of reactions with 25 mM M_5, 25 mM ^{18}O-G_2M_5 in 20 mM NaAc pH 5.2, and 0.1 g/L BSA at 8 °C using WT *Me*Man5A. Transglycosylation products are shown in A but not in B. Both (**A**,**B**) show detection of oligosaccharide products (M_2–M_4). Transglycosylation products with degree of polymerization (DP) 7–8 (M_7 and M_8) were detected with WT *Me*Man5A (**A**) but not with W240A/W281A (**B**). An increase in M_2–M_4 peak areas was observed from 1 through 5 h for both WT *Me*Man5A and W240A/W281A. The M_6 minor peak in spectra A and B is an impurity in the M_5 used as substrate. The spectrum in (**C**) shows detection of ^{18}O-labeled transglycosylation products with DP 9–10 resulting from usage of ^{18}O-labeled G_2M_5 as acceptor by WT. The ^{18}O-DP6 and ^{18}O-DP8 minor peaks in spectrum (**C**) are impurities in the ^{18}O-G_2M_5 used as acceptor. The observed monoisotopic sodium adduct m/z is shown next to each labeled peak in spectra A, B, and C. The theoretical m/z (Na-adducts) of these compounds are M_2, 365.11; M_3, 527.16; M_4, 689.21; M_5, 851.27; M_6, 1013.32; M_7, 1175.37; M_8, 1337.42; ^{18}O-G_2M_5, 1177.37; ^{18}O-DP6, 1015.32; ^{18}O-DP8, 1339.42; ^{18}O-DP9, 1501.48; ^{18}O-DP10, 1663.53.

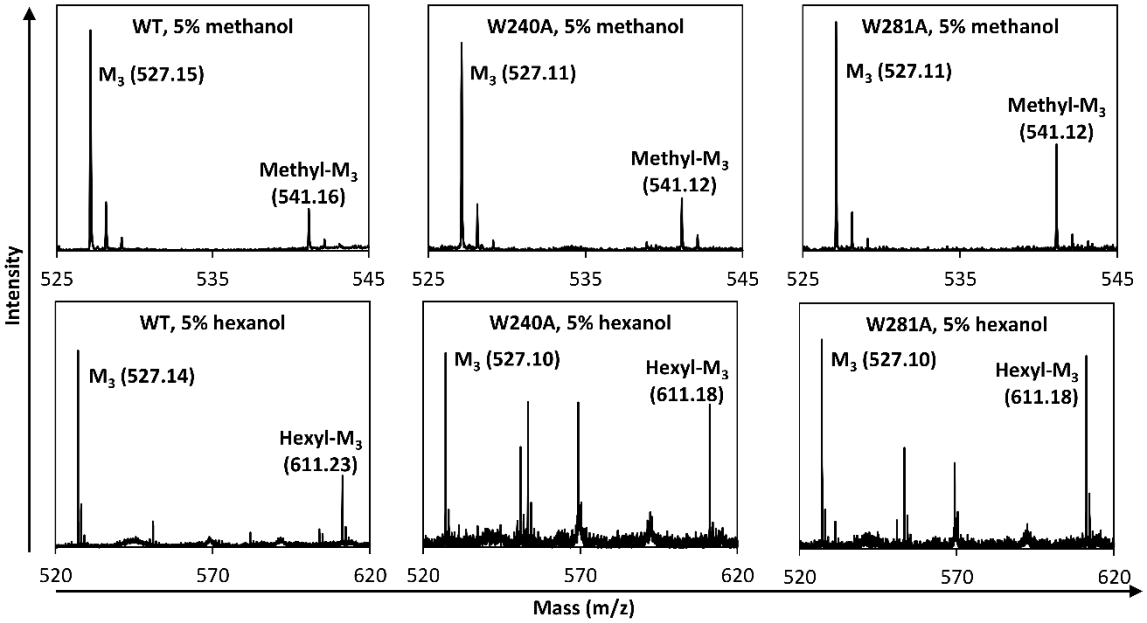

Figure 3. MALDI-TOF MS spectra of reactions with 5 mM M_5 and 5% (*v*/*v*) methanol (top row) or hexanol (bottom row), respectively, for 1 h, with WT *Me*Man5A (left column), W240A (middle column) and W281A (right column). The spectra show detection of mannotriose (M_3) and either methyl mannotrioside (methyl-M_3) or hexyl mannotrioside (hexyl-M_3). The observed monoisotopic sodium adduct m/z is shown next to each labeled peak. The theoretical m/z of these compounds (Na-adducts) are M_3, 527.16; methyl-M_3, 541.09; hexyl-M_3, 611.25.

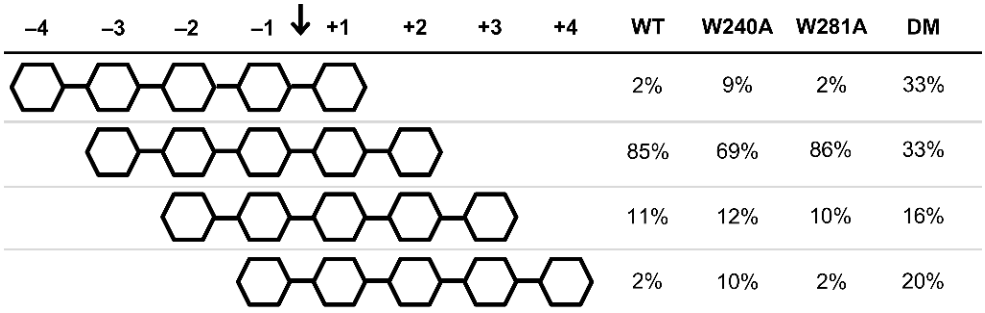

Figure 4. Productive binding mode preferences with M_5 by WT *Me*Man5A, W240A, W281A, and W240A/W281A (DM). Subsites −4 through +4 are indicated, with hydrolysis of the glycosidic bond between subsites −1 and +1 shown by the arrow. Mannose units are shown as hexagons.

2.4. Enzyme Kinetics

With galactomannan (LBG) as substrate, WT *Me*Man5A has a k_{cat} of 332 ± 5 s^{-1} and a K_M of 0.75 ± 0.05 g/L (Table 2). Compared to WT *Me*Man5A, W240A has a 3.2-fold lower k_{cat} and 1.7-fold higher K_M, whereas W281A has a 2.7-fold reduction of k_{cat} but no change in K_M (Table 2). W240A/W281A has a lower k_{cat} value than W240A and W281A, as well as an even higher K_M value than W240A, resulting in the most pronounced decrease (25-fold) of k_{cat}/K_M compared to WT for any of the substituted variants (Table 2). Thus, even though the W281A substitution on its own does not affect K_M, substituting both W240 and W281 causes a greater increase in K_M than substituting W240 alone.

Table 2. Kinetic parameters of locust bean galactomannan (LBG), mannotetraose (M_4), and mannopentaose (M_5) hydrolysis by WT *Me*Man5A, W240A, W281A, and W240A/W281A.

Enzyme Variant	LBG k_{cat} (s^{-1})	LBG K_M ($g \cdot L^{-1}$)	LBG k_{cat}/K_M ($g \cdot L^{-1} \cdot s^{-1}$)	M_4 k_{cat}/K_M ($s^{-1} \cdot mM^{-1}$)	M_5 k_{cat}/K_M ($s^{-1} \cdot mM^{-1}$)
WT	332 ± 5	0.75 ± 0.05	446 ± 30	0.71 ± 0.05	36 ± 2
W240A	105 ± 3	1.3 ± 0.1	83 ± 9	0.18 ± 0.02	2.8 ± 0.5
W281A	121 ± 3	0.73 ± 0.1	165 ± 15	0.55 ± 0.08	17 ± 3
W240A/W281A	66.4 ± 18	3.7 ± 0.4	18 ± 5	0.23 ± 0.01	0.84 ± 0.03

Also, with M_4 and M_5, k_{cat}/K_M decreased for the substituted variants, similarly with LBG. With M_5, there is a 13-fold decrease in k_{cat}/K_M comparing WT *Me*Man5A and W240A, whereas the W281A substitution only causes a 2-fold decrease (Table 2). The greatest decrease in k_{cat}/K_M with M_5 was again observed with W240A/W281A (43-fold), and it is even more pronounced than with LBG (Table 2). The reduced productive M_5-binding in the +2 subsite of W240A/W281A (Figure 4) could be compensated by more distal subsites (−4 and +3) when the higher-DP substrate LBG is used, as indicated in the WT *Me*Man5A structure [29]. This may be a common feature among GH5 endo-mannanases. In the case of *Tr*Man5A, the loss of glycan interaction in the +2 subsite, provided by arginine (R171), was also suggested to be compensated by distal subsites [7]. A 50-fold increase in k_{cat}/K_M between M_4 and M_5 for WT *Me*Man5A (Table 2) strongly suggests that substrate-binding in at least five subsites is required for efficient hydrolysis. These subsites are −3 to +2 (Figure 4, Section 2.3).

Taken together, the kinetic data show that both W240 and W281 are needed for catalytic efficiency. Interpretation of the previous apo crystal structure [29] indicates that W240 possibly interacts with a mannosyl unit in the +2 subsite, while the W281 is too distant, requiring movement for such interaction simultaneously as W240 (Figure 1A). To address the roles of these residues, it was important to further investigate their potential glycan binding properties and flexibility, as outlined in the two following sections.

2.5. Tryptophan Flexibility and Glycan Interactions

To investigate the possible flexibility of the W281 side-chain and its potential role in interactions with glycans, *Me*Man5A was studied by Nuclear Magnetic Resonance (NMR) spectroscopy. In the ^{1}H–^{15}N heteronuclear single quantum coherence (HSQC) spectra of WT *Me*Man5A, 13 tryptophan indole N–H peaks could be detected, as expected from the *Me*Man5A sequence [29]. The chemical shifts of the W281 indole N–H were identified by comparing tryptophan indole N–H peaks in ^{1}H–^{15}N HSQC spectra of WT *Me*Man5A and W281A, for which the W281 indole was absent (Figure S3).

Different glycans were then added to study their possible interactions with W281 and the other five surface-exposed tryptophans in the active site cleft (Figure 1A). Upon the addition of M_2 and M_3, no significant change in the W281 chemical shift was observed, indicating that W281 does not interact with these shorter glycans or change its orientation in response to their binding. However, a change in the W281 chemical shift was observed with G_2M_5 added (Figure 5), indicating that W281 senses or directly binds G_2M_5. The assignment of the W281 peak in the G_2M_5-bound state was based on a comparison of the spectral changes of the tryptophan indole region between the unbound enzyme state and the M_2-, M_3-, and G_2M_5-bound states (Figure 5). The increasing length of the glycans from M_2 to M_3 to G_2M_5 is expected to result in gradual changes in the spectrum for tryptophans that respond to glycan binding. Indeed, as seen in Figure 5, this was observed for several tryptophan indole peaks: peak 1 (moving 'north'), 2 ('southwest'), 3, and 5 (merging by moving 'northeast' and 'southwest', respectively), while peak 10 shows a more complex pattern and peaks 4, 6, 7, 8, 11, 12, and 13 do not exhibit any significant changes. As a result, we can assign the boxed peak in the spectrum of the G_2M_5-bound state to W281 (Figure 5). The result that chemical-shift changes are observed for six peaks (1, 2, 3, 5, 10, and W281) is

logical considering that this number matches the number of tryptophans in the active site of *Me*Man5A: W42 in subsite −3, W79 in subsite −2, W337 in subsite −1, W205 in subsite +1, and W240 and W281 in subsite +2 [29] (Figure 1A).

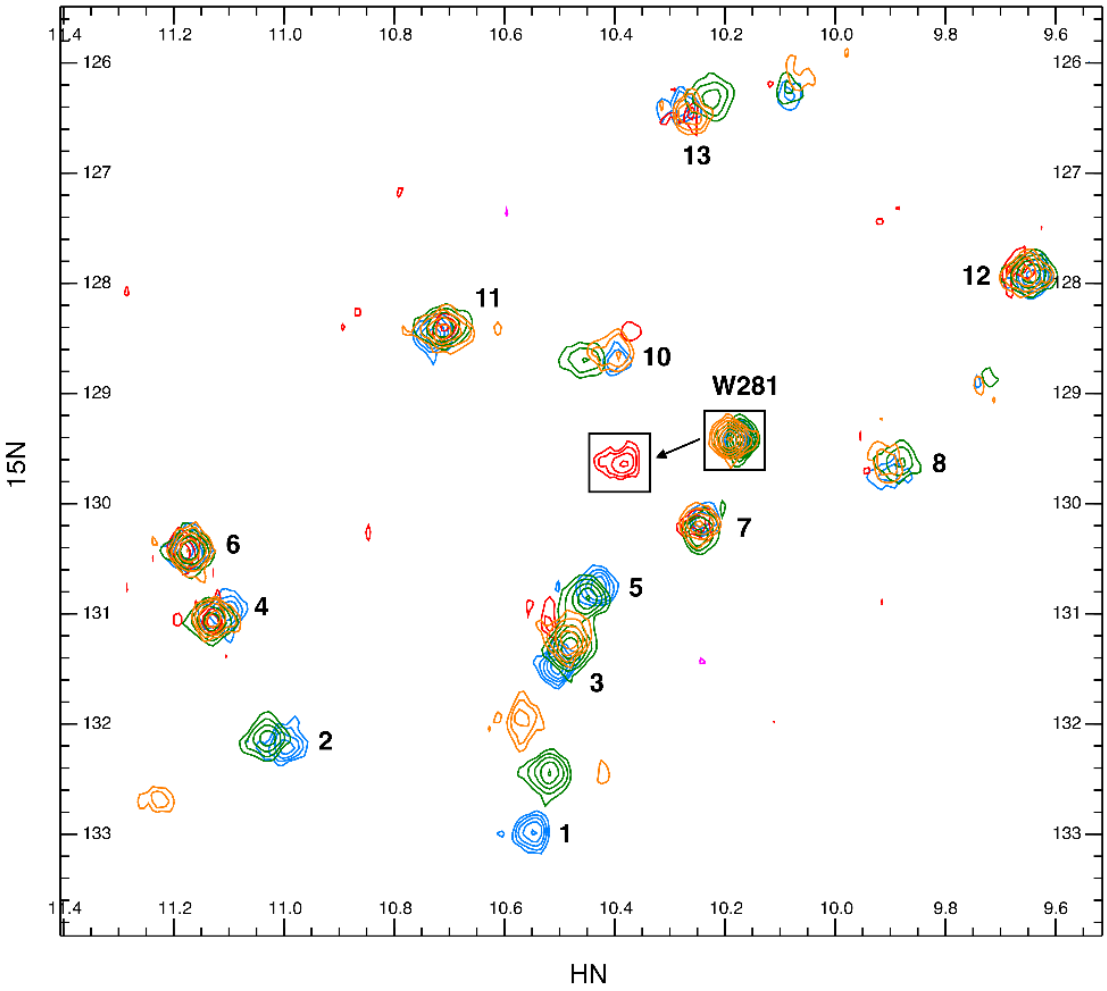

Figure 5. ^{1}H–^{15}N HSQC NMR spectra of WT *Me*Man5A showing the tryptophan indole amide region of the spectra without added ligand (blue) as well as with M_2 (green), M_3 (orange) or G_2M_5 (red) added. Numbers correspond to unassigned tryptophan indoles, while the W281 peak is indicated within squares. A change in the W281 chemical shift upon adding G_2M_5 is shown with the arrow.

The transverse relaxation rates (R_2) for W281 in the unbound and M_2-bound states of the enzyme are similar but significantly lower than those for the other tryptophans (Table 3), indicating a higher degree of intrinsic flexibility on the pico- to nanosecond time scale. However, with the addition of G_2M_5, an increase in R_2 was observed for W281, indicating reduced flexibility of W281 when the enzyme binds G_2M_5 (Table 3), possibly because of the direct interaction of W281 with G_2M_5. This observation agrees with the result that W281 exhibits significant chemical shift changes only when *Me*Man5A binds G_2M_5 but not the shorter oligosaccharides. The current NMR results support the previous hypothesis based on X-ray crystallography that movement of the W281 would be required for W281 to interact with mannosyl units in the +2 subsite [29].

Table 3. R_2 relaxation data values without substrate (apo) and with M_2 or G_2M_5 as added glycans, for residues identified as tryptophans in NMR studies of WT *Me*Man5A.

Residue	R_2 (apo)	R_2 (M_2)	R_2 (G_2M_5)
Trp #1	21.2 ± 1.55	21.3 ± 1.65	n.d. [a]
Trp #2	25.7 ± 1.73	23.3 ± 1.21	n.d. [a]
Trp #3	19.7 ± 0.52	21.8 ± 1.01	n.d. [a]
Trp #4	24.0 ± 2.79	26.4 ± 1.75	29.1 ± 4.81
Trp #5	20.3 ± 1.01	21.8 ± 0.94	n.d. [a]
Trp #6	22.1 ± 1.08	25.4 ± 1.83	27.2 ± 2.12
Trp #7	23.5 ± 2.06	23.3 ± 1.44	22.0 ± 3.02
Trp #8	31.2 ± 4.04	28.1 ± 3.34	n.d. [a]
Trp #9 (W281)	12.0 ± 0.31	12.4 ± 0.27	18.2 ± 1.82
Trp #10	31.6 ± 7.59	31.1 ± 5.17	19.1 ± 7.92
Trp #11	22.5 ± 1.11	24.1 ± 1.86	23.3 ± 4.16
Trp #12	20.8 ± 1.40	21.1 ± 0.73	19.6 ± 2.35
Trp #13	30.9 ± 7.79	27.2 ± 4.38	24.3 ± 3.21

[a] Not determinable.

2.6. Glycan Interaction and Flexibility Analyzed by Molecular Dynamics Simulation

Molecular dynamics (MD) simulation further supported the occurrence of W281 flexibility in the apo structure of *Me*Man5A. Simulation using the *Me*Man5A crystal structure (PDB: 2C0H) at 40 °C over 800 ns indicated limited flexibility of the loop harboring W281, with an average backbone RMSD from the crystal structure of 0.94 Å for residues 278–293 (compared to 0.98 Å for the whole protein) but interestingly, a maximum of 2.7 Å (compared to 1.5 Å for the whole protein). By contrast, the side chain of W281 showed significant flexibility. The center of the six-membered ring portion of W281 was at least 2 Å away from the crystal structure position 87% of the time, with an average of 4.9 Å and a maximum of 11.2 Å; the distance distribution is shown in Figure S4 and a pictorial representation of the ensemble in Figure S5. Two extreme positions of W281 in the apo-enzyme are shown in Figure S6A,B. Further insight was gained by performing MD simulation with ligand (M_6) bound in the −3 to +3 subsites. The ligand was positioned by the superimposition of the *Me*Man5A apo-structure (PDB: 2C0H) with the StMandC complex structure (PDB: 4Y7E) (Figure 1A). The MD simulation indicated that W281 flexibility was reduced, as was the loop backbone (maximum loop RMSD 2.0 Å and maximum ring center distance 5.9 Å). Simulation over 70 ns revealed W281 mainly in one position, and this was distinctly different (2.7 Å) from the (apo) crystal structure (Figure 1B, Figures S4, S5 and S6C). Minor fluctuations occurred, but with the center of the W281 six-membered ring within 2 Å of its average position 96% of the time and at a distance of 4.1 ± 0.5 Å from the C1 of the mannosyl located in subsite +2 (Figure 1B) (4.3 ± 0.4 Å from the C4 of subsite +3; ± indicates standard deviation). The average position of W281 with the ligand appears to provide stacking interactions with the mannosyl unit in subsite +2. It should be noted that the W240 side-chain remained rigid at hydrogen bond distance to the subsite +2 mannosyl C2-OH throughout the simulation. This hydrogen bond was also suggested when *Me*Man5A was superimposed with an M_2-complex structure of β-mannanase *Tr*Man5A [29]. Our current MD data reveal that the majority of residues within 4Å from the ligand had low flexibility (RMSD < 1.2 Å). However, two residues were strikingly flexible in the apo simulation, Q132 and Y279 (RMSD 3.3 Å and 2.9 Å, respectively). Q132 was previously predicted to H-bond to a mannosyl unit if it occupied subsite −3 and the conserved (GH5) Y279 is exposed in the active site where it interacts with the nucleophile [29]. In accordance with their location in the structure, both Q132 and Y279 could interact with M_6 in the complex simulation and thus showed reduced flexibility (RMSD 1.8 and 0.6 Å, respectively) compared to that observed in the apo-enzyme simulation. Taken together, the MD data provide further mechanistic insight into the substrate-binding behavior of *Me*Man5A.

3. Discussion

Positively numbered (+) subsite residues may have important roles not only in hydrolysis but also in transglycosylation, as shown for different GHs [22]. Among them are GH5_7 β-mannanases [7,8,10] not previously investigated for GH5_10 β-mannanases. The present work further underlines the functional significance of aglycone residues in GHs. The aglycone region architecture of GH5_10 *Me*Man5A studied in this paper differs from the previously studied GH5_7 β-mannanases. *Me*Man5A contains two semi-conserved tryptophans (W240 and W281) in the +2 subsite, with W281 located in a loop. We found that these tryptophans play a significant role in hydrolysis and transglycosylation, providing glycan binding in subsite +2. Mutational analysis revealed that substitutions W240A and W281A reduce *Me*Man5A's catalytic efficiency towards LBG and mannooligosaccharides, although their roles differ.

Structural analysis of the superimposed apo *Me*Man5A and StMandC M_6-bound crystal structures indicates that W240 interacts with the substrate, whereas movements of W281 and its loop would require this interaction (Figure 1A). Findings in the NMR and MD studies of *Me*Man5A strongly support the crucial role of structural flexibility in the loop containing W281 and in the side chain for substrate-binding in subsite +2, as shown in Figure 1B. The transverse relaxation rates provided in this text show that W281 is more flexible in comparison to other tryptophans in the apoprotein (Table 3). Flexibility is also evident at the ns timescales accessible by molecular dynamics (Figures S4 and S5), although the observed conformational states are not necessarily representative of the ms timescale dynamics probed by analysis of the transverse relaxation rates. Simulations of the enzyme with and without M_6 show that the W240 side-chain remains rigid and that the indole NH is within hydrogen bonding distance from the +2 subsite mannosyl C2-OH. Since this hydroxyl configuration differs from glucose, W240 likely helps to provide mannose specificity in the +2 subsite. Mannosyl specificity in the +2 subsite occurs at least in some other GH5 mannanases as well, such as for the GH5_7 β-mannanase*Tr*Man5A, which uses a mannose-interacting arginine (R171) which is semi-conserved in subfamily GH5_7 β-mannanases [7,34].

When analyzing *Me*Man5A in the presence of the glycan G_2M_5, our NMR data clearly demonstrate that W281 in the +2 subsite senses or directly binds this glycan, as evidenced by the observed change in chemical shift (Figure 5). Furthermore, the ^{15}N relaxation data reveal a significant reduction in the flexibility of W281 upon G_2M_5 binding (Table 3), potentially indicating a direct interaction with the substrate. MD simulations also support these observations, showing that W281 exhibits reduced flexibility compared to the apo-enzyme and adopts a more suitable position for stacking interaction with the mannosyl in the +2 subsite when complexed with M_6 (Figure 1B, Figures S4, S5 and S6). This adjustment includes the movement of both the loop backbone and the side chain of W281. Loop dynamics might possibly also be involved in glycan binding in the GH5_8 β-mannanase StMandC, where a subsite +2 tryptophan (situated on a different loop compared to ours) provides substrate interaction [35]. For another type of hemicellulase, GH11 xylanases, there is a prominent thumb loop that can be flexible, and its polar residues could be involved in both initial substrate-binding in negative subsites and product release [36]. This may, however, vary in GH11 because, in some cases, this loop is rigid. Surface loops involving hydrophobic residues may be involved in substrate interactions in various types of enzymes [37] and other GHs [35,38,39]. Furthermore, examples of single-exposed tryptophans involved in initial glycan binding for carbohydrate-active enzymes have been observed, as in the case of a glucan interacting carbohydrate-binding module from a glucanase [40].

Taken together, biochemical analysis, NMR experiments, and MD simulation data strongly suggest that not only the rigid W240 interacts with glycans in the +2 subsite but also W281, for which loop and side-chain movements are required for simultaneous substrate contact, which, in turn, reduces the flexibility. We investigated two states of *Me*Man5A using MD simulation, the apo-enzyme and when bound to M6, but not the transition in

between. W281 was shown to be positioned to suitably provide stacking interaction, while W240 provides mannose specificity in the +2 subsite (Figure 1B). Considering that W281 is flexible in the apo-enzyme and is exposed close to the edge of the binding cleft, it could be speculated that W281 might be involved in substrate capture and contributes to the positioning of the glycan in the active site cleft where the rigid W240 is positioned for binding in the bottom of the cleft.

Transglycosylation experiments carried out herein indicate that W281 participates in glycan acceptor interactions during transglycosylation. The significance of W281 in acceptor interactions is further evident from the substantial decrease in transglycosylation capacity with saccharide acceptors upon W281 substitution (Table 1). Substituting W240 also leads to a notable reduction in transglycosylation with saccharide acceptors, and complete elimination of saccharide transglycosylation capacity is observed in W240A/W281A (Table 1). This suggests that W240 and W281 contribute to glycan acceptor-binding. Hydrophobic residues such as tryptophans are important in glycan interactions [41], an example of which is the mutational analysis of a GH31 α-glucosidase [42]. However, the substitutions W240A and W281A do not impact transglycosylation with alcohol acceptors, as demonstrated by the production of alkyl mannosides using methanol and hexanol as acceptors at the tested concentration (Figure 3). For the GH5_7 β-mannanase *Tr*Man5A, the +2 subsite arginine, R171, appears to interact with saccharide acceptors, as its substitution abolishes transglycosylation with saccharides while maintaining activity with alcohols [7,18]. Thus, both polar and non-polar residues in the +2 subsite of GH5 mannanases may play significant roles in glycan acceptor interactions. Considering the semi-conservation of R171 in *Tr*Man5A and W240/W281 in *Me*Man5A within subfamilies GH_7 and GH5_10, respectively, similar functions may potentially extend to many other GH5 mannanases and are of interest for targeted mutations to increase the transglycosylation yields of these enzymes when utilizing alcohols as acceptors for generation of novel glycosides.

4. Materials and Methods

4.1. Carbohydrates and Media

Mannose (M_1), mannobiose (M_2), mannotriose (M_3), mannotetraose (M_4), mannopentaose (M_5), 6^3,6^4-α-D-galactosyl-mannopentaose (G_2M_5), and locust bean galactomannan (LBG) were obtained from Megazyme (Bray, Ireland). Lysogeny broth (LB) medium for *Escherichia coli* [43] was prepared as follows: 10 g/L tryptone, 5 g/L yeast extract, and 10 g/L sodium chloride. Growth media for *Pichia pastoris* were prepared as follows, according to the EasySelect *Pichia* Expression Kit manual (Thermo Fisher Scientific, Waltham, MA, USA). Yeast peptone-dextrose (YPD) medium: 10 g/L yeast extract, 20 g/L peptone, and 20 g/L glucose, with 20 g/L agar added for YPD plates. Buffered glycerol-complex (BMGY) and methanol-complex (BMMY) media: 10 g/L yeast extract, 20 g/L peptone, 100 mM potassium phosphate pH 6.0, 3.4 g/L yeast nitrogen base without amino acids and ammonium sulfate, 10 g/L ammonium sulfate, and 40 µg/l biotin and 1% (*v*/*v*) glycerol (BMGY) or 0.5% (*v*/*v*) methanol (BMMY). Buffered minimal glycerol (BMGH) or methanol (BMMH) media: same as BMGY and BMMY but without yeast extract and peptone. ^{15}N-ammonium sulfate was obtained from Cortecnet (Voisins-Le-Bretonneux, Yvelines, France).

4.2. Construction of Enzyme Variants

Mutagenesis was performed according to the Quikchange™ PCR protocol (Agilent Technologies, Santa Clara, CA, USA) using *Pfu* polymerase. For creating the +2 subsite-substituted *Me*Man5A single mutants *Me*Man5A-W240A (in text referred to as W240A) and *Me*Man5A-W281A (in text referred to as W281A), the pPICZαB plasmid containing the wild-type *Me*Man5A gene (GenBank accession number AJ271365.2) encoding the wild-type sequence *Me*Man5A (in text also referred to as WT, as in wild-type) [28] without a polyhistidine tag (pPICZαB-*Me*Man5A) was extracted from *E. coli* TOP10 cells (Thermo Fisher Scientific) using the JETSTAR Plasmid Midiprep kit (Genomed, Löhne, Germany). This plasmid was used as a template for site-directed mutagenesis using primer pairs corresponding

to each of the +2 subsite mutations (Table S1), creating the pPICZαB-*Me*Man5A-W240A and pPICZαB-*Me*Man5A-W281A plasmids, respectively. To create the double mutant *Me*Man5A-W240A/W281A (referred to as A240/W281A), the pPICZαB-*Me*Man5A-W240A plasmid was used as template for PCR amplification with the primer pair corresponding to the W281A mutation (Table S1) to create the pPICZαB-*Me*Man5A-W240A/W281A plasmid. The amplified PCR products were treated with *Dpn*I (Thermo Fisher Scientific) and transformed into *E. coli* TOP10 (Thermo Fisher Scientific) by electroporation according to the manufacturer's recommendations. Mutations were confirmed by plasmid sequencing of the coding region (Eurofins Genomics, Ebersberg, Germany).

4.3. Transformation of Pichia Pastoris and β-Mannanase Assay

Plasmids were extracted and purified from *E. coli* TOP10 cells using the JETSTAR Plasmid Midiprep kit (Genomed), linearized using *Sac*I, and purified by ethanol precipitation. Electrocompetent *P. pastoris* cells were prepared and electroporated with 5–10 µg of linearized plasmid with genes encoding WT *Me*Man5A, W240A, W281A, or W240A/W281A, according to the EasySelect *Pichia* Expression Kit manual (Thermo Fisher Scientific). Transformants were streaked on YPD plates with 1M sorbitol and 100 µg/mL zeocin (Thermo Fisher Scientific) and incubated for 3 days at 30 °C. Isolated transformants were cultured and screened for β-mannanase activity using the 3,5-dinitrosalicylic acid (DNS) assay described previously [44]. Briefly, 40 µL of appropriately diluted culture supernatant was added to 360 µL of 5 g/L LBG in 50 mM sodium citrate buffer, pH 5.2, and incubated for 10 min at 40 °C. The reaction was stopped by adding 600 µL DNS and boiling for 5 min. Absorbance was measured at 540 nm and converted into enzyme activity using a mannose standard curve.

4.4. Expression in Pichia Pastoris

Expression was performed as described in the EasySelect *Pichia* Expression Kit manual (Thermo Fisher Scientific) and guided by previous studies [27–29]. Recombinant *P. pastoris* cells with genes encoding WT *Me*Man5A, W240A, W281A, or W240A/W281A were streaked on YPD plates with 100 µg/mL zeocin (Thermo Fisher Scientific) and incubated for 3 days at 30 °C. Single colonies from each plate were used to inoculate 50 mL BMGY in 250 mL baffled flasks and incubated overnight at 30 °C with 150 rpm shaking. Each cell pellet was collected by centrifugation (4000 rpm, 20 min) and resuspended in 500 mL BMMY in 2 L baffled flasks. The cells were incubated for 6 days at 17 °C with 150 rpm shaking, and methanol was added to a final concentration of 0.5% every 12 h. When β-mannanase activity reached a plateau in the culture supernatant, cells were pelleted by centrifugation, and the supernatants were collected for purification. The expression of ^{15}N-labeled WT *Me*Man5A and W281A was performed as described above except BMGH and BMMH with $(^{15}NH_4)_2SO_4$ as nitrogen source was used instead of BMGY and BMMY, respectively, and expression was performed for 9 days at 17 °C.

4.5. Enzyme Purification

The expression culture supernatants were concentrated, and the buffer was changed to purification loading buffer (50 mM Na_2HPO_4, 300 mM NaCl, 5 mM imidazole, pH 8.0) using an Amicon 8400 stirred cell (Merck Millipore, Darmstadt, Germany). WT *Me*Man5A, W240A, W281A, and W240A/W281A were purified using immobilized metal ion affinity chromatography (IMAC) using a BioLogic DuoFlow™ chromatography system (Bio-Rad, Hercules, CA, USA), where the samples were applied to a 1 mL Ni-NTA Superflow cartridge (Qiagen, Hilden, Germany) and eluted with a 5–250 mM imidazole gradient using a flow rate of 1 mL/min. Protein purity was analyzed with SDS-PAGE [26]. WT *Me*Man5A and variants W240A, W281A, and W240A/W281A migrated as single bands at approx. 39 kDa, which is the expected molecular weight. Binding to the column thus was achieved likely due to the high number of His on the surface of the *Me*Man5A structure [29]. Enzyme concentrations were measured using the BCA™ Protein Assay Kit (Thermo Fisher

Scientific). After purification, the buffer was changed to 50 mM sodium citrate, pH 5.2, using an Amicon 8050 stirred cell (Merck Millipore, Billerica, MA, USA).

4.6. Basic Enzyme Characterization

To determine specific activity towards LBG, the β-mannanase activity of WT *Me*Man5A (50 nM), W240A (110 nM), W281A (93 nM), and W240A/W281A (243 nM) was measured using the DNS assay in 20 mM sodium citrate buffer, pH 5.2. The same assay was used to determine pH optima but with buffers adjusted to pH 4.5–6.0. Temperature stability was determined by storing enzyme aliquots in 50 mM sodium citrate, pH 5.2, at room temperature, 30 °C and 40 °C, as well as at 40 °C with 0.1 mg/mL Bovine Serum Albumin (BSA, Sigma-Aldrich, St. Louis, MO, USA) for up to 24 h with activity assayed at 0, 2, 4, 6, 8, and 24 h. Activities are presented as average ± deviation.

4.7. Enzyme Kinetics

For determining the k_{cat} and K_M of LBG hydrolysis, the DNS assay was used but with varying LBG concentrations and using 20 min incubation time. WT *Me*Man5A (50 nM), W240A (110 nM), W281A (93 nM), or W240A/W281A (243 nM) were incubated with LBG solutions in 50 mM sodium citrate buffer, pH 5.2, with LBG concentrations of 0.25, 0.50, 1.0, 2.5, 5.0, 7.5, and 10 g/L at 40 °C for 20 min with 0.1 mg/mL BSA added. Duplicate incubations were performed for each LBG concentration. Response linearity from 0 to 20 min was assayed by sampling after 0, 10, 20, and 30 min. Hydrolysis rates were obtained for each substrate concentration, and k_{cat} and K_M values were calculated by non-linear regression using Prism 6 (GraphPad Software, La Jolla, CA, USA).

For determining the catalytic efficiency (k_{cat}/K_M) of M_4 hydrolysis, 125 µM of M_4 was incubated in duplicate with WT *Me*Man5A (100 nM), W240A (100 nM), W281A (100 nM), or W240A/W281A (500 nM) for 0–2 h in 50 mM sodium citrate buffer, pH 5.2, at 40 °C with 0.1 mg/mL BSA added. The k_{cat}/K_M ratio of M_5 hydrolysis was determined in the same way except with 1 nM of WT *Me*Man5A, 10 nM of W240A, 3 nM of W281A, or 200 nM of W281A/W240A. Samples were withdrawn at regular time intervals, boiled for 5 min, and analyzed with high-performance anion exchange chromatography with pulsed amperometric detection (HPAEC-PAD) using a DX-500 system and a CarboPac PA-200 column (Thermo Fisher Scientific). The rate of hydrolysis was plotted using the equation $\ln([S]_0/[S]_t) = k^*t$, where $[S]_0$ is the initial substrate concentration and $[S]_t$ is the substrate concentration at time t [8,45–47]. The k_{cat}/K_M ratio was calculated by dividing rate (k) by enzyme concentration. Kinetic values are presented as average ± deviation.

4.8. Product Formation and Productive Binding Mode Preferences

To gain insight into the product formation from M_5 conversion, WT *Me*Man5A (5 nM), W240A (50 nM), W281A (10 nM), or W240A/W281A (800 nM) were incubated with 1 mM M_5 for 0–1 h (WT *Me*Man5A, W240A, and W281A) or 0–20 min (W240A/W281A) in 20 mM sodium acetate buffer, pH 5.2, at 40 °C with 0.1 g/L BSA added. Samples were taken every 15 min (WT *Me*Man5A, W240A, and W281A) or every 5 min (W240A/W281A) and analyzed with HPAEC-PAD as described above. Saccharide concentrations are presented as average ± deviation.

In the hydrolysis of oligosaccharides, several different binding modes can generate products with the same degree of polymerization (DP) (e.g., binding M_5 from subsite −3 to +2 and −2 to +3, which both produce M_2 and M_3). In order to differentiate between the productive binding modes of M_5 and determine the relative preference of *Me*Man5A for each mode, 0.8 mM M_5 was incubated with WT *Me*Man5A (39 nM), W240A (32 nM) or W281A (26 nM) for 0–4 h or with W240A/W281A (53 nM) for 0–24 h in $H_2{}^{18}O$, following the procedure of previous studies [7,8,33,48]. Incubations were performed in 93% $H_2{}^{18}O$ with 1 mM sodium citrate buffer, pH 5.2. A low temperature (8 °C) was used to limit spontaneous ^{18}O incorporation [33]. During hydrolysis with $H_2{}^{18}O$, ^{18}O is incorporated into the glycone product but not the aglycone product. By analyzing the samples with MADLI-ToF MS,

the ratio between labeled (^{18}O) and unlabeled (^{16}O) products with the same DP can be calculated, allowing the differentiation of binding modes generating otherwise identical products [33]. Samples were taken at regular time intervals and analyzed with MALDI-TOF MS using a 4700 Proteomics Analyzer (Applied Biosystems, Foster City, CA, USA) in positive reflector mode with a laser intensity of 5500. Samples (0.5 µL) were spotted on a stainless-steel target plate and dried by heating. Each sample was then covered in 1 µL matrix solution (10 mg/mL 2,5-dihydroxybenzoic acid) and again dried by heating. To generate a spectrum, 50 subspectra with 20 shots on each were collected from a sample. The data was analyzed using Data Explorer version 4.5 (Applied Biosystems). Samples were also analyzed with HPAEC-PAD as described above to determine product concentrations, and this data was combined with ^{18}O/^{16}O product ratios to calculate the relative preference of each *Me*Man5A variant for each M_5 binding mode as described in a previous study [7].

4.9. Transglycosylation with Saccharides and Alcohols as Acceptors

The formation of transglycosylation products was analyzed by incubating WT *Me*Man5A (20 nM), W240A (129 nM), W281A (21 nM), or W240A/W281A (424 nM) with 5 mM M_5 in 20 mM sodium acetate buffer, pH 5.2, at 40 °C for 0–6 h with 0.1 g/L BSA added. Samples were taken every hour and analyzed with MALDI-TOF MS as described above.

Transglycosylation was further studied using a saccharide, which is non-hydrolyzable by *Me*Man5A, G_2M_5, as an acceptor. To analyze G_2M_5 incorporation into oligosaccharide products, G_2M_5 was labeled with ^{18}O in its reducing end as described previously [8], resulting in 89% labeling as determined by MALDI-TOF MS peak areas of ^{16}O- and ^{18}O-G_2M_5. An amount of 25 mM of ^{18}O-G_2M_5 and 25 mM of M_5 was then incubated with 100 nM of WT *Me*Man5A in 20 mM sodium acetate buffer, pH 5.2, for 0–96 h at 8 °C with 0.1 g/L BSA added. Samples were taken at 0, 1, 3, 24, 48, 72, and 96 h and analyzed with MALDI-TOF MS as described above. As a control reaction, the same reaction mixture and parameters were used, except ^{18}O-G_2M_5 was omitted.

To analyze transglycosylation capacity with alcohols as acceptors, WT *Me*Man5A (25 nM) was initially screened with 5 mM M_5 and either methanol (5% or 10% *v*/*v*), propargyl alcohol (5% *v*/*v*), or hexanol (5% *v*/*v*). The reactions were incubated for 0–1 h at 40 °C. W240A (250 nM) or W281A (50 nM) using methanol and hexanol as acceptors and for 5 h when using propargyl alcohol. The hexanol was dried with a 3Å molecular sieve (Sigma-Aldrich, St. Louis, MO, USA) for at least 24 h before use. Samples were taken every hour and analyzed with MALDI-TOF MS in duplicate as described above.

4.10. NMR Spectroscopy

The flexibility and glycan interactions of the W281 side-chain were studied using nuclear magnetic resonance (NMR) spectroscopy. First, the W281 indole ^{1}H/^{15}N cross-peak in the ^{1}H-^{15}N heteronuclear single quantum coherence (HSQC) spectrum was assigned by mutation, i.e., by comparing the spectra of WT *Me*Man5A (0.23 mM) and W281A (0.18 mM), recorded at a static magnetic field strength of B_0 = 14.1 T. The spectral widths were 8445.9 Hz, covered by 2048 points, and 2066.7 Hz, covered by 128 points in the ^{1}H and ^{15}N dimensions, respectively. Second, ^{1}H-^{15}N HSQC spectra of WT *Me*Man5A in its unbound form and bound to M_2, M_3, and G_2M_5 were recorded at B_0 = 11.7 T. The spectral widths were 8012.8 Hz, covered by 2048 points, and 1550 Hz, covered by 128 points in the ^{1}H and ^{15}N dimensions, respectively. The spectral widths were 8012.8 Hz, covered by 2048 points, and 1550 Hz, covered by 128 points in the ^{1}H and ^{15}N dimensions, respectively. Third, longitudinal (R_1) and transverse (R_2) ^{15}N relaxation experiments [49,50] targeting the tryptophan indole ^{15}N spins were recorded on WT *Me*Man5A in the unbound, M_2-, M_3-, and G_2M_5-bound states using 20 mM ligand and B_0 = 11.7 T. The spectral widths were 8012.8 Hz, covered by 1344 points, and 1550 Hz, covered by 128 points in the ^{1}H and ^{15}N dimensions, respectively. A total of 10 data points were recorded with relaxation delays in the range of 0–1.25 s and 0–0.12 s for R_1 and R_2, respectively. Values were presented as averages ± standard deviation. The ^{15}N relaxation-compensated Carr–Purcell–

Meiboom–Gill (CPMG) relaxation dispersion experiments [51–53] were carried out on WT *Me*Man5A in the unbound state, using a constant relaxation delay of 40 ms and 20 refocusing frequencies ranging from 50–1000 Hz. In all experiments, the temperature was 25 °C, and the carrier frequencies were placed on the water in the ^{1}H dimension and in the middle of the amide region in the ^{15}N dimension.

All spectra were processed using NMRPipe [54] with linear prediction in the indirect dimension to extend the interferograms to twice the original size, followed by a squared cosine window function. Spectra were assigned using the CcpNmr [55] suite. Peaks were integrated, and relaxation decays were fitted using PINT [56].

4.11. Molecular Dynamics Simulation

The W281 flexibility and glycan interactions were studied by molecular dynamics (MD) simulation. The apo crystal structure of *Me*Man5A (PDB: 2C0H) was used as the starting structure for the simulation of the apoprotein, as well as the simulation of the protein complexed with mannohexaose (M_6). The structure file used for simulating the ligand interaction was generated by structural superimposition of apo *Me*Man5A and the nucleophile substituted E273A GH5_8 β-mannanase StMandC co-crystallized with M_6 (PDB: 4Y7E) [35] resulting in a position of the mannohexaose ligand in subsite −3 to +3 of *Me*Man5A. The partial mannosyl occupancy in subsite −4 of StMandC was excluded. There were two mannose moieties occupying the −1 subsite of the StMandC crystal structure, one internal in distorted $B_{2,5}$ boat conformation, and one reducing end mannosyl moiety, which was excluded. The protein was prepared by removing residues 15–17 from the N terminal, creating a disulfide bridge between Cys-192 and Cys-259, removing the sulfate ion and crystal waters, and determining the protonation state of the residues at pH 6.5 by the standard protocol of the H++ server followed by manual inspection (His-31, 32, 51, 71, 112, 117, 154, 208, 252, 258, 277, 284, 293, 313, 353, and 360 were doubly protonated; His-81 and 135 were protonated at N^{δ}; His-197 was protonated at N^{ε}; Glu-181 and Asp-245 were neutral (protonated); both terminals were charged).

The Amber ff14SB force field was employed for the protein, TIP3P was used for water, and GLYCAM06 was used for the ligand [57,58]. All simulations were performed at constant temperature (40 °C), maintained by the velocity rescaling thermostat, and at constant pressure (1 bar), maintained by the Parrinello–Rahman barostat. Long-range electrostatics were treated by the Particle Mesh Ewald method with a cutoff of 0.9 nm and a grid spacing of 0.12 nm. All bond lengths were constrained by the LINCS algorithm as implemented in GROMACS 2018, and a time-step of 2 fs was used.

The following equilibration protocol was employed: energy minimization with restraints on all protein-heavy atoms, followed by 0.5 ns MD with position restraints on all protein-heavy atoms, followed by 1.5 ns MD with position restraints (harmonic potential with force constant 500 kJ mol^{-1} nm^{-2}) on all C_{α} atoms and an artificial 3 Å distance restraint between Lys301:NZ and Asp247:OD2 (to try to stabilize a plausible salt bridge replacing the Lys301-sulphate interaction in the crystal structure). For the complex, an additional long equilibration run of 60 ns was performed, in which the internal conformation of the ligand was fixed by applying distance restraints on all internal C-C distances (flat-bottomed harmonic potentials with force constant 5000 kJ mol^{-1} nm^{-2} and a flat region of ±0.5 Å of the initial structure to allow vibration but not torsional swapping). Without the restrained equilibration, the ligand tended to slightly change conformation after ~13 ns and lose some interactions with the protein. After the restrained equilibration, longer stable periods were observed in several independent unrestrained runs (up to 77 ns) before the conformational change of the ligand occurred (the change itself indicates a possible issue with the GLYCAM06 force field, but this was not further investigated as the internal conformational variation of the ligand was decided to be out of the scope in this study).

After equilibration, all restraints were removed in the production simulations. For the apoprotein, a simulation time of 800 ns was used, during which no significant distortion

from the crystal structure was observed (average RMSD 0.98 Å). For the complex, only 70 ns of the simulation was used in the analysis to avoid the internal conformational change of the M_6 ligand, but we validated that essentially identical results regarding protein conformation would have been obtained if, instead, the longer restrained runs had been analyzed.

5. Conclusions

In conclusion, the present study provides mechanistic insight into the role of subsite +2 residues in hydrolysis and transglycosylation by GH5 β-mannanases. Based on the results of the present study, we propose that W240 and W281 in *Me*Man5A are involved in substrate- and acceptor-binding, where the flexibility of the loop backbone and W281 side-chain flexibility is important for W281 interaction. We have shown that W240 and W281 contribute to the catalytic efficiency of *Me*Man5A in different ways, where the rigid W240 provides binding specificity, and W281 is indicated to have a role in contributing to stacking positioning of the glycan chain for catalysis. Furthermore, the W240A and W281A substitutions reduced or eliminated transglycosylation with saccharides as acceptors but did not significantly affect alcoholysis with methanol or hexanol as acceptors.

The propensity for *Me*Man5A to utilize methanol, propargyl alcohol, and hexanol as acceptors would be of interest to future studies. The presented results further support the general involvement of +2 subsite residues in GH-catalyzed transglycosylation using saccharides as acceptors, and that removal of saccharide binding affinity in this subsite reduces or abolishes acceptor competition when using alcohols as acceptors. This makes *Me*Man5A an interesting enzyme to exploit in future applications of enzymatic synthesis.

Supplementary Materials: The following supporting information can be downloaded at https://www.mdpi.com/article/10.3390/catal13091281/s1, Table S1: Sequences and properties of the primers used for the W240A and W281A substitutions. Figure S1: MALDI-TOF MS spectrum showing detection of unlabeled oligosaccharide products in a reaction with WT *Me*Man5A. Figure S2: MALDI-ToF spectra of reactions with 5 mM M_5 and WT *Me*Man5A after 5 h at 40 °C with and without propargyl alcohol as control. Figure S3: ^{1}H-^{15}N HSQC NMR spectra of WT *Me*Man5A and W281A. Figure S4: Histogram showing the distribution of the distance of the center of the W281 ring relative to its position in the crystal structure for the apo simulation and the complex simulation. Figure S5: Variation of the W281 position in the apo simulation and the complex simulation. Figure S6: Simulation results of *Me*Man5A with mannohexaose ligand.

Author Contributions: Conceptualization, J.M., M.A., P.S. and H.S.; methodology, S.B., J.M., O.S., M.W., U.W., P.S., M.A. and H.S.; validation S.B., J.M., M.W. and O.S.; formal analysis, S.B., J.M., O.S., M.W., P.S. and H.S.; investigation, S.B., J.M., O.S., M.W., U.W. and P.S.; resources, H.S.; data curation S.B., J.M., O.S., M.W., U.W., P.S., M.A. and H.S.; writing—original draft, S.B., J.M., O.S., M.W. and P.S.; writing—review and editing, U.W., M.A. and H.S.; visualization, S.B., J.M., O.S., M.W., P.S. and H.S.; supervision; U.W., M.A. and H.S.; project administration, H.S.; funding acquisition, H.S. All authors have read and agreed to the published version of the manuscript.

Funding: This research was funded by grants to H.S. from Formas (grant number 942-2016-117), the Carl Trygger Foundation (grant number 16:452), and the Swedish Research Council (grant number 2019-05605) and by a grant to M.A. from the Swedish Research Council (grant number 621-2014-5815).

Data Availability Statement: The data presented in this study are available in the article or the supplementary material.

Conflicts of Interest: The authors declare no conflict of interest.

References

1. Dawood, A.; Ma, K. Applications of microbial β-mannanases. *Front. Bioeng. Biotechnol.* **2020**, *8*, 598630. [CrossRef] [PubMed]
2. Henrissat, B. A classification of glycoside hydrolases based on amino acid sequence similarities. *Biochem. J.* **1991**, *280*, 309–316. [CrossRef] [PubMed]
3. Lombard, V.; Golaconde Ramulu, H.; Drula, E.; Coutinho, P.M.; Henrissat, B. The carbohydrate-active enzymes database (CAZy) in 2013. *Nucleic Acids Res.* **2014**, *42*, D490–D495. [CrossRef] [PubMed]

4. Aspeborg, H.; Coutinho, P.; Wang, Y.; Brumer, H.; Henrissat, B. Evolution, substrate specificity and subfamily classification of glycoside hydrolase family 5 (GH5). *BMC Evol. Biol.* **2012**, *12*, 186. [CrossRef]
5. Rye, C.S.; Withers, S.G. Glycosidase mechanisms. *Curr. Opin. Chem. Biol.* **2000**, *4*, 573–580. [CrossRef]
6. Bissaro, B.; Monsan, P.; Faure, R.; O'Donohue, M.J. Glycosynthesis in a waterworld: New insight into the molecular basis of transglycosylation in retaining glycoside hydrolases. *Biochem. J.* **2015**, *467*, 17–35. [CrossRef]
7. Rosengren, A.; Hägglund, P.; Anderson, L.; Pavon-Orozco, P.; Peterson-Wulff, R.; Nerinckx, W.; Stålbrand, H. The role of subsite +2 of the Trichoderma reesei β-mannanase TrMan5A in hydrolysis and transglycosylation. *Biocatal. Biotransform.* **2012**, *30*, 338–352. [CrossRef]
8. Rosengren, A.; Reddy, S.K.; Sjöberg, J.S.; Aurelius, O.; Logan, D.T.; Kolenová, K.; Stålbrand, H. An Aspergillus nidulans β-mannanase with high transglycosylation capacity revealed through comparative studies within glycosidase family 5. *Appl. Microbiol. Biotechnol.* **2014**, *98*, 10091–10104. [CrossRef]
9. Butler, S.J.; Birgersson, S.; Wiemann, M.; Arcos-Hernandez, M.; Stålbrand, H. Transglycosylation by β-mannanase TrMan5A variants and enzyme synergy for synthesis of allyl glycosides from galactomannan. *Process Biochem.* **2022**, *112*, 154–166. [CrossRef]
10. Dilokpimol, A.; Nakai, H.; Gotfredsen, C.H.; Baumann, M.J.; Nakai, N.; Abou Hachem, M.; Svensson, B. Recombinant production and characterisation of two related GH5 endo-β-1,4-mannanases from Aspergillus nidulans FGSC A4 showing distinctly different transglycosylation capacity. *Biochim. Biophys. Acta* **2011**, *1814*, 1720–1729. [CrossRef]
11. Couturier, M.; Roussel, A.; Rosengren, A.; Leone, P.; Stålbrand, H.; Berrin, J.G. Structural and biochemical analyses of glycoside hydrolase families 5 and 26 β-(1,4)-mannanases from Podospora anserina reveal differences upon manno-oligosaccharide catalysis. *J. Biol. Chem.* **2013**, *288*, 14624–14635. [CrossRef] [PubMed]
12. Srivastava, P.K.; Kapoor, M. Production, properties, and applications of endo-β-mannanases. *Biotechnol. Adv.* **2017**, *35*, 1–19. [CrossRef] [PubMed]
13. Lundqvist, J.; Teleman, A.; Junel, L.; Zacchi, G.; Dahlman, O.; Tjerneld, F.; Stålbrand, H. Isolation and characterization of galactoglucomannan from spruce (*Picea abies*). *Carbohydr. Polym.* **2002**, *48*, 29–39. [CrossRef]
14. Scheller, H.V.; Ulvskov, P. Hemicelluloses. *Annu. Rev. Plant Biol.* **2010**, *61*, 263–289. [CrossRef] [PubMed]
15. Voiniciuc, C. Modern mannan: A hemicellulose's journey. *New Phytol.* **2022**, *234*, 1175–1184. [CrossRef]
16. Agger, J.W.; Zeuner, B. Bio-based surfactants: Enzymatic functionalization and production from renewable resources. *Curr. Opin. Biotechnol.* **2022**, *78*, 102842. [CrossRef]
17. Arcos-Hernandez, M.; Naidjonoka, P.; Butler, S.J.; Nylander, T.; Stålbrand, H.; Jannasch, P. Thermoresponsive Glycopolymers Based on Enzymatically Synthesized Oligo-β-Mannosyl Ethyl Methacrylates and N-Isopropylacrylamide. *Biomacromolecules* **2021**, *22*, 2338–2351. [CrossRef]
18. Morrill, J.; Månberger, A.; Rosengren, A.; Naidjonoka, P.; von Freiesleben, P.; Krogh, K.B.R.M.; Bergquist, K.E.; Nylander, T.; Nordberg Karlsson, E.; Adlercreutz, P.; et al. β-Mannanase-catalyzed synthesis of alkyl mannooligosides. *Appl. Microbiol. Biotechnol.* **2018**, *102*, 5149–5163. [CrossRef]
19. Wang, Y.; Vilaplana, F.; Brumer, H.; Aspeborg, H. Enzymatic characterization of a glycoside hydrolase family 5 subfamily 7 (GH5_7) mannanase from Arabidopsis thaliana. *Planta* **2014**, *239*, 653–665. [CrossRef]
20. Brusa, C.; Belloy, N.; Gérard, D.; Muzard, M.; Dauchez, M.; Plantier-Royon, R.; Rémond, C. Exploring the aglycone subsite of a GH11 xylanase for the synthesis of xylosides by transglycosylation reactions. *J. Biotechnol.* **2018**, *272–273*, 56–63. [CrossRef]
21. Eide, K.B.; Lindbom, A.R.; Eijsink, V.G.H.; Norberg, A.L.; Sørlie, M. Analysis of productive binding modes in the human chitotriosidase. *FEBS Lett.* **2013**, *587*, 3508–3513. [CrossRef] [PubMed]
22. Abdul Manas, N.H.; Md. Ilias, R.; Mahadi, N.M. Strategy in manipulating transglycosylation activity of glycosyl hydrolase for oligosaccharide production. *Crit. Rev. Biotechnol.* **2018**, *38*, 272–293. [CrossRef] [PubMed]
23. Teze, D.; Zhao, J.; Wiemann, M.; Kazi, Z.G.A.; Lupo, R.; Zeuner, B.; Vuillemin, M.; Rønne, M.E.; Carlström, G.; Duus, J.O.; et al. Rational Enzyme Design without Structural Knowledge: A Sequence-Based Approach for Efficient Generation of Transglycosylases. *Chem. Eur. J.* **2021**, *27*, 10323–10334. [CrossRef] [PubMed]
24. Ueda, M.; Hirano, Y.; Fukuhara, H.; Naka, Y.; Nakazawa, M.; Sakamoto, T.; Ogata, Y.; Tamada, T. Gene cloning, expression, and X-ray crystallographic analysis of a β-mannanase from Eisenia fetida. *Enzym. Microb. Technol.* **2018**, *117*, 15–22. [CrossRef] [PubMed]
25. Schröder, R.; Wegrzyn, T.F.; Sharma, N.N.; Atkinson, R.G. LeMAN4 endo-β-mannanase from ripe tomato fruit can act as a mannan transglycosylase or hydrolase. *Planta* **2006**, *224*, 1091–1102. [CrossRef]
26. Xu, B.; Hägglund, P.; Stålbrand, H.; Janson, J.C. endo-β-1,4-Mannanases from blue mussel, Mytilus edulis: Purification, characterization, and mode of action. *J. Biotechnol.* **2002**, *92*, 267–277. [CrossRef]
27. Xu, B.; Muñoz, I.G.; Janson, J.C.; Ståhlberg, J. Crystallization and X-ray analysis of native and selenomethionyl β-mannanase Man5A from blue mussel, Mytilus edulis, expressed in Pichia pastoris. *Acta Cryst.* **2002**, *D58*, 542–545. [CrossRef]
28. Xu, B.; Sellos, D.; Janson, J.C. Cloning and expression in Pichia pastoris of a blue mussel (*Mytilus edulis*) β-mannanase gene. *Eur. J. Biochem.* **2002**, *269*, 1753–1760. [CrossRef]
29. Larsson, A.M.; Anderson, L.; Xu, B.; Muñoz, I.G.; Usón, I.; Janson, J.C.; Stålbrand, H.; Ståhlberg, J. Three-dimensional crystal structure and enzymic characterization of β-mannanase Man5A from blue mussel *Mytilus edulis*. *J. Mol. Biol.* **2006**, *357*, 1500–1510. [CrossRef]
30. Lobo-da-Cunha, A. Structure and function of the digestive system in molluscs. *Cell Tissue Res.* **2019**, *377*, 475–503. [CrossRef]

31. Mizutani, K.; Tsuchiya, S.; Toyoda, M.; Nanbu, Y.; Tominaga, K.; Yuasa, K.; Takahashi, N.; Tsuji, A.; Mikami, B. Structure of β-1,4-mannanase from the common sea hare Aplysia kurodai at 1.05 Å resolution. *Acta Cryst.* **2012**, *F68*, 1164–1168. [CrossRef]
32. Kim, M.K.; An, Y.J.; Song, J.M.; Jeong, C.S.; Kang, M.H.; Kwon, K.K.; Lee, Y.H.; Cha, S.S. Structure-based investigation into the functional roles of the extended loop and substrate-recognition sites in an endo-β-1,4-D-mannanase from the Antarctic springtail, *Cryptopygus antarcticus*. *Proteins* **2014**, *82*, 3217–3223. [CrossRef]
33. Hekmat, O.; Lo Leggio, L.; Rosengren, A.; Kamarauskaite, J.; Kolenova, K.; Stålbrand, H. Rational engineering of mannosyl binding in the distal glycone subsites of *Cellulomonas fimi* endo-β-1,4-mannanase: Mannosyl binding promoted at subsite −2 and demoted at subsite−3. *Biochemistry* **2010**, *49*, 4884–4896. [CrossRef]
34. Sabini, E.; Schubert, H.; Murshudov, G.; Wilson, K.S.; Siika-Aho, M.; Penttilä, M. The three-dimensional structure of a *Trichoderma reesei* β-mannanase from glycoside hydrolase family 5. *Acta Cryst.* **2000**, *D56*, 3–13. [CrossRef] [PubMed]
35. Kumagai, Y.; Yamashita, K.; Tagami, T.; Uraji, M.; Wan, K.; Okuyama, M.; Yao, M.; Kimura, A.; Hatanaka, T. The loop structure of Actinomycete glycoside hydrolase family 5 mannanases governs substrate recognition. *FEBS J.* **2015**, *282*, 4001–4014. [CrossRef] [PubMed]
36. Gagné, D.; Narayanan, C.; Nguyen-Thi, N.; Roux, L.D.; Bernard, D.N.; Brunzelle, J.S.; Couture, J.-F.; Agarwal, P.K.; Doucet, N. Ligand binding enhances millisecond conformational exchange in xylanase B2 from Streptomyces lividans. *Biochemistry* **2016**, *55*, 4184–4196. [CrossRef]
37. Smith, C.A.; Stewart, N.K.; Toth, M.; Vakulenko, S.B. Structural insights into the mechanism of carbapenemase activity of the OXA-48 β-lactamase. *Antimicrob. Agents Chemother.* **2019**, *63*, 10. [CrossRef]
38. Madhuprakash, J.; Singh, A.; Kumar, S.; Sinha, M.; Kaur, P.; Sharma, S.; Podile, A.R.; Singh, T.P. Structure of chitinase D from *Serratia proteamaculans* reveals the structural basis of its dual action of hydrolysis and transglycosylation. *Int. J. Biochem. Mol. Biol.* **2013**, *4*, 166–178.
39. Wu, M.; Bu, L.; Vuong, T.V.; Wilson, D.B.; Crowley, M.F.; Sandgren, M.; Ståhlberg, J.; Beckham, G.T.; Hansson, H. Loop motions important to product expulsion in the *Thermobifida fusca* glycoside hydrolase family 6 cellobiohydrolase from structural and computational studies. *J. Biol. Chem.* **2013**, *288*, 33107–33117. [CrossRef]
40. Miki, A.; Inaba, S.; Maruno, T.; Kobayashi, Y.; Oda, M. Tryptophan introduction can change β-glucan binding ability of the carbohydrate-binding module of endo-1,3-β-glucanase. *Biosci. Biotechnol. Biochem.* **2017**, *81*, 951–957. [CrossRef]
41. Kiessling, L.L.; Diehl, R. CH-π Interactions in Glycan Recognition. *ACS Chem. Biol.* **2021**, *16*, 1884–1893. [CrossRef] [PubMed]
42. Song, K.M.; Okuyama, M.; Nishimura, M.; Tagami, T.; Mori, H.; Kimura, A. Aromatic residue on β→α loop 1 in the catalytic domain is important to the transglycosylation specificity of glycoside hydrolase family 31 α-glucosidase. *Biosci. Biotechnol. Biochem.* **2013**, *72*, 1759–1765. [CrossRef]
43. Bertani, G. Studies on lysogenesis. I. The mode of phage liberation by lysogenic *Escherichia coli*. *J. Bacteriol.* **1951**, *62*, 293–300. [CrossRef] [PubMed]
44. Stålbrand, H.; Siika-Aho, M.; Tenkanen, M.; Viikari, L. Purification and characterization of two β-mannanases from Trichoderma reesei. *J. Biotechnol.* **1993**, *29*, 229–242. [CrossRef]
45. Suganuma, T.; Matsuno, R.; Ohnishi, M.; Hiromi, K. A study of the mechanism of action of Taka-amylase A on linear oligosaccharides by product analysis and computer simulation. *J. Biochem.* **1978**, *84*, 293–316. [CrossRef]
46. Matsui, I.; Ishikawa, K.; Matsui, E.; Miyairi, S.; Fukui, S.; Honda, K. Subsite structure of Saccharomycopsis α-amylase secreted from *Saccharomyces cerevisiae*. *J. Biochem.* **1991**, *109*, 566–569. [CrossRef]
47. Hogg, D.; Pell, G.; Dupree, P.; Goubet, F.; Martin-Orué, S.M.; Armand, S.; Gilbert, H.J. The modular architecture of Cellvibrio japonicus mannanases in glycoside hydrolase families 5 and 26 points to differences in their role in mannan degradation. *Biochem. J.* **2003**, *371*, 1027–1043. [CrossRef]
48. Bågenholm, V.; Reddy, S.K.; Bouraoui, H.; Morrill, J.; Kulcinskaja, E.; Bahr, C.M.; Aurelius, O.; Rogers, T.; Xiao, Y.; Logan, D.T.; et al. Galactomannan catabolism conferred by a polysaccharide utilization locus of *Bacteroides ovatus*: Enzyme synergy and crystal structure of a β-mannanase. *J. Biol. Chem.* **2017**, *292*, 229–243. [CrossRef] [PubMed]
49. Koerdel, J.; Skelton, N.J.; Akke, M.; Palmer, A.G.; Chazin, W.J. Backbone dynamics of calcium-loaded calbindin D9k studied by two-dimensional proton-detected nitrogen-15 NMR spectroscopy. *Biochemistry* **1992**, *31*, 4856–4866. [CrossRef]
50. Farrow, N.A.; Muhandiram, R.; Singer, A.U.; Pascal, S.M.; Kay, C.M.; Gish, I.G.; Shoelson, S.E.; Pawson, T.; Forman-Kay, J.D.; Kay, L.E. Backbone Dynamics of a Free and a Phosphopeptide-Complexed Src Homology 2 Domain Studied by 15N NMR Relaxation. *Biochemistry* **1994**, *33*, 5984–6003. [CrossRef]
51. Carr, H.Y.; Purcell, E.M. Effects of diffusion on free precession in nuclear magnetic resonance experiments. *Phys. Rev.* **1954**, *94*, 630–638. [CrossRef]
52. Meiboom, S.; Gill, D. Modified spin-echo method for measuring nuclear relaxation times. *Rev. Sci. Instrum.* **1958**, *29*, 688–691. [CrossRef]
53. Loria, J.P.; Rance, M.; Palmer, A.G.R. A relaxation-compensated Carr-Purcell-Meiboom-Gill sequence for characterizing chemical exchange by NMR spectroscopy. *J. Am. Chem. Soc.* **1999**, *121*, 2331–2332. [CrossRef]
54. Delaglio, F.; Grzesiek, S.; Vuister, G.W.; Zhu, G.; Pfeifer, J.; Bax, A. NMRPipe: A multidimensional spectral processing system based on UNIX pipes. *J. Biomol. NMR* **1995**, *6*, 277–293. [CrossRef] [PubMed]
55. Vranken, W.F.; Boucher, W.; Stevens, T.J.; Fogh, R.H.; Pajon, A.; Llinas, M.; Ulrich, E.L.; Markley, J.L.; Ionides, J.; Laue, E.D. The CCPN data model for NMR spectroscopy: Development of a software pipeline. *Proteins* **2005**, *59*, 687–696. [CrossRef] [PubMed]

56. Ahlner, A.; Carlsson, M.; Jonsson, B.H.; Lundström, P. PINT: A software for integration of peak volumes and extraction of relaxation rates. *J. Biomol. NMR* **2013**, *56*, 191–202. [CrossRef]
57. Maier, J.A.; Martinez, C.; Kasavajhala, K.; Wickstrom, L.; Hauser, K.E.; Simmerling, C. ff14SB: Improving the Accuracy of Protein Side Chain and Backbone Parameters from ff99SB. *J. Chem. Theory Comput.* **2015**, *11*, 3696–3713. [CrossRef]
58. Allouche, A. Software News and Updates Gabedit—A Graphical User Interface for Computational Chemistry Softwares. *J. Comput. Chem.* **2012**, *32*, 174–182. [CrossRef]